Progress in Organic Coatings 97 (2016) 28–36

Contents lists available at ScienceDirect

Progress in Organic Coatings

journal homepage: www.elsevier.com/locate/porgcoat

Silver-functionalized methyl-silica hybrid materials as antibacterial coatings on surgical-grade stainless steel

R. Procaccini[a], A. Bouchet[b], J.I. Pastore[b], C. Studdert[c], S. Ceré[a], S. Pellice[a,*]

[a] Instituto de Investigación en Ciencia y Tecnología de Materiales (INTEMA), UNMdP-CONICET, Av. Juan B. Justo 4302, 7600 Mar del Plata, Argentina
[b] Grupo de Procesamiento Digital de Imágenes. Universidad Nacional de Mar del Plata, Facultad de Ingeniería. Juan B. Justo 4302, 7600 Mar del Plata, Argentina
[c] Instituto de Investigaciones Biológicas (IIB), UNMdP-CONICET, Funes 3250, 7600 Mar del Plata, Argentina

ARTICLE INFO

Article history:
Received 17 November 2015
Received in revised form 19 February 2016
Accepted 7 March 2016

Keywords:
Sol-gel
Silver nanoparticles
EIS
Synchrotron SAXS
XPS

ABSTRACT

Development of new materials enriched with noble metal ions, such as silver, cobalt or copper, is of great interest in the field of commercial and medical products due to its action against fungus and bacteria. Although a large number of products are chemically active against microorganisms, they are usually limited to fabrics for medical bandages and sportswear in order to avoid, respectively, infections and odors. On the other hand, sol-gel technology becomes the preparation of hybrid materials possible with introduction of different components, as inorganic salts or organic additives within its structure bringing up the possibility to develop functional materials for different purposes.

In this work, the development of an antibacterial coating for metallic substrates is presented. The coating consists in a hybrid organic-inorganic sol-gel material doped with silver. The relation between the structure of the hybrid matrix, aggregation state of silver ions, and biocide behavior is analyzed as a function of the densifying thermal treatment. Sol-gel materials were synthesized through hydrolytic condensation, in acidic conditions, of tetraethoxysilane (TEOS) and methyl-triethoxysilane (MTES). Silica nanoparticles were added in order to give a mechanical reinforcement and silver nitrate as the supplier of Ag^+ ions. Coatings were deposited on 316L stainless steel and microscope glass slides by the dip-coating process at a constant withdrawal rate and densified at 50, 150 and 450 °C. X-ray photoelectron spectroscopy, small angle X-ray spectroscopy and electrochemical impedance spectroscopy were used as characterization techniques in order to elucidate silver aggregation and its influence on the structural evolution of the hybrid matrix, as a function of the thermal treatment. At the same time, the biocide behavior, as a function of silver state, particles size and thermal treatment, was studied by inhibitory halo identification on *Escherichia-coli* cultures in agar diffusion tests.

1. Introduction

The development of new functional materials capable to provide an effective antibacterial activity has a big demand from the contemporary society. This fact is mainly due to the easy propagation that microorganisms have in this globally connected world with a continuously growing population. The action of viruses and bacteria often presents serious damages that can turn in economic losses or even in loss of human lives. In this field, silver is a well-known biocide component due to the activity of Ag^+ ions [1–5]. Silver ions have an effective action against bacteria life inhibiting their DNA replication process, increasing the permeability of the cytoplasmic membrane and inhibiting the respiratory enzymes, causing asphyxia of the bacteria. Thus, silver is effectively used as the active additive, against fungus and bacteria, both in medical devices and in commercial textile products, like sportswear and burn bandages [6–12]. In the same way, the use of silver as antibacterial additive for thin solid coatings could provide a powerful tool in order to set a major obstacle to the spread of infections; specially, in the environments where people is highly exposed to infectious microorganisms as, e.g., public toilets, public transport and hospitals. Nowadays, also for surgical prosthesis and orthopedic devices, silver based coatings are in focus for the prevention of periprosthetic infections is a scientific topic of strong activ-

* Corresponding author.
E-mail address: spellice@fi.mdp.edu.ar (S. Pellice).

http://dx.doi.org/10.1016/j.porgcoat.2016.03.012
0300-9440/

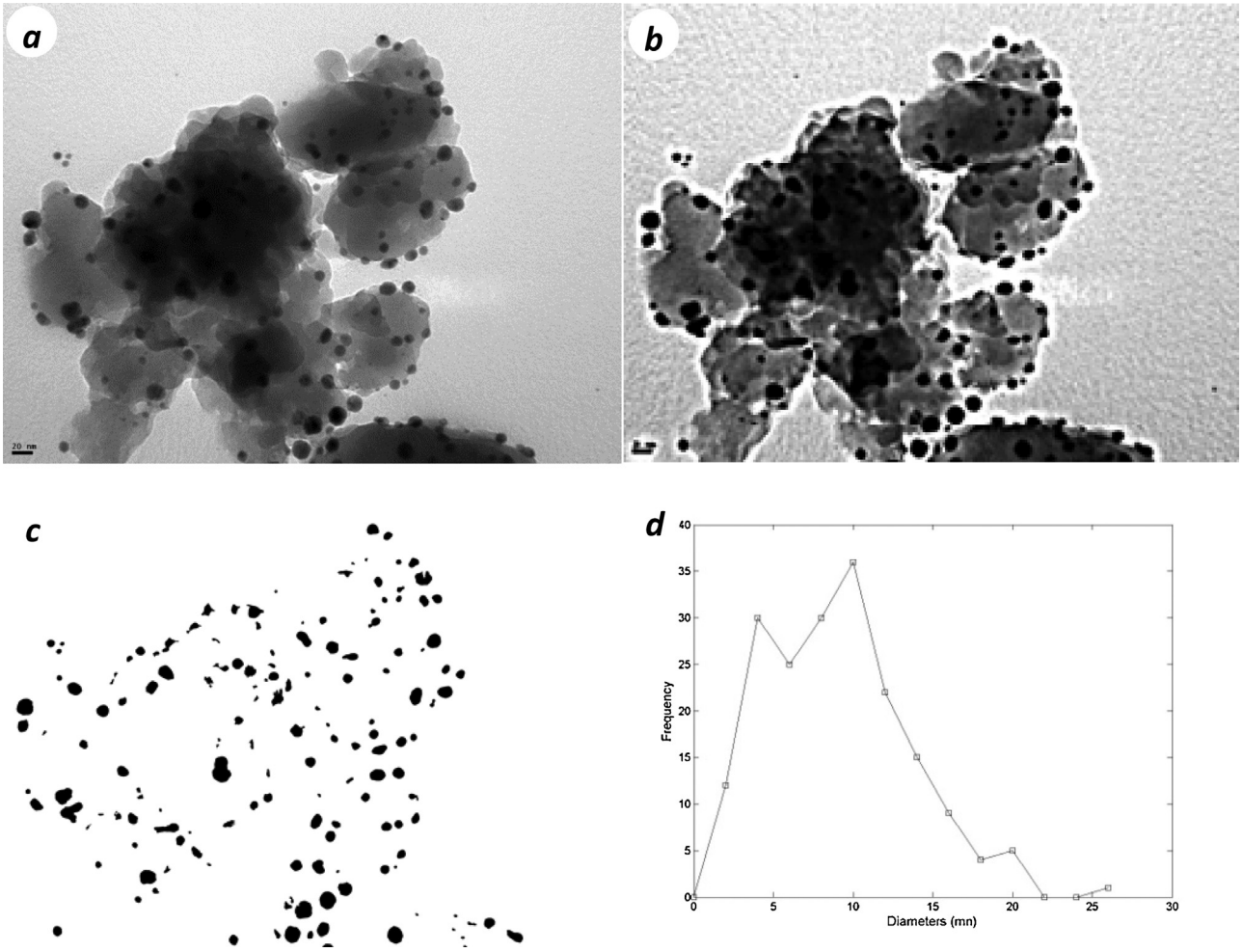

Fig. 1. Algorithm for detection and measurement of size distribution of silver particles. (a) Original image, (b) spectrally filtered image, (c) binary image and (d) size distribution of silver nanoparticles. The size of the bars in figures (a) and (c) represent 20 nm.

ity [13–18]. Certainly, although stainless steel does not present antibacterial properties by itself, it is a material that present optimal conditions in term of sterility and economical suitability as a material for surgical devices [19–21].

A promising method to produce such silver functionalized thin coatings comes from the sol-gel chemistry, which is a worldwide subject of study as a method to produce functional coatings [22,23]. Sol-gel chemistry, as a very versatile method of synthesis, allows the development of hybrid organic-inorganic materials with incorporation of a wide variety of external components, as particles, organic compounds, inorganic salts, etc. Then, through this method, it is possible to combine design a tailored material with both mechanical and functional properties [24]. This feature becomes it in a particularly promising approach to produce efficient antibacterial thin coatings where the biocide functionality derives from silver action. In this kind of materials, silver works by way of the diffusion of Ag^+ ions, or its smallest clusters, through the structure of the containing matrix towards the external surface, where microorganisms are reached. Then, both the development of a sol-gel network with an extremely open structure or the agglomeration process of silver, to form particles that would remain entrapped in the matrix, are features that could strongly limit the resulting antibacterial performance. It was seen that for sol-gel structures without an enough crosslinking density, lixiviation of silver ions may be extremely fast, producing an initial burst release and limiting the long-term antibacterial performance [25–27]. Furthermore, Ag^+ ions present a strong tendency to be reduced in the chemical conditions proper of the sol–gel process, resulting in an agglomeration process that carries to a rise of silver nanoparticles. Certainly, the growth of small silver clusters and nanoparticles is nearly impossible to avoid when the doped sol-gel coating is applied and a thermal treatment is performed [27,28]. So, in order to develop a hybrid organic–inorganic thin coating, providing a controlled silver release rate and avoiding an initial burst release effect and dangerous cytotoxic conditions, both the matrix structure and the agglomeration process of silver should be optimized.

The goal of this work is, in one hand, to deal with the in-situ self-development of silver nanoparticles from is reduction from Ag+ ions added in a hybrid organic-inorganic matrix of a thin coatings; this phenomenon is thermal-dependent and its behavior is of interest both in the fields of optical, electrical and antibacterial materials. On the other hand, the remaining of silver as Ag+ ions, avoiding its self-arrangement in silver nanoparticles, is mainly important for the antibacterial effect. In this sense, the evolution of silver aggregates inside hybrid coatings deposited onto surgical grade stainless steel is analyzed in the present work.

In this work the study of the oxidative state of silver, and the agglomeration phenomena inside of a silica-methyl hybrid matrix reinforced with silica nanoparticles was addressed. The resulting relationship between the aggregation state of silver, the structure of the hybrid matrix and the antibacterial effect in the developed sol–gel coatings was also studied. Through the use of a synchrotron

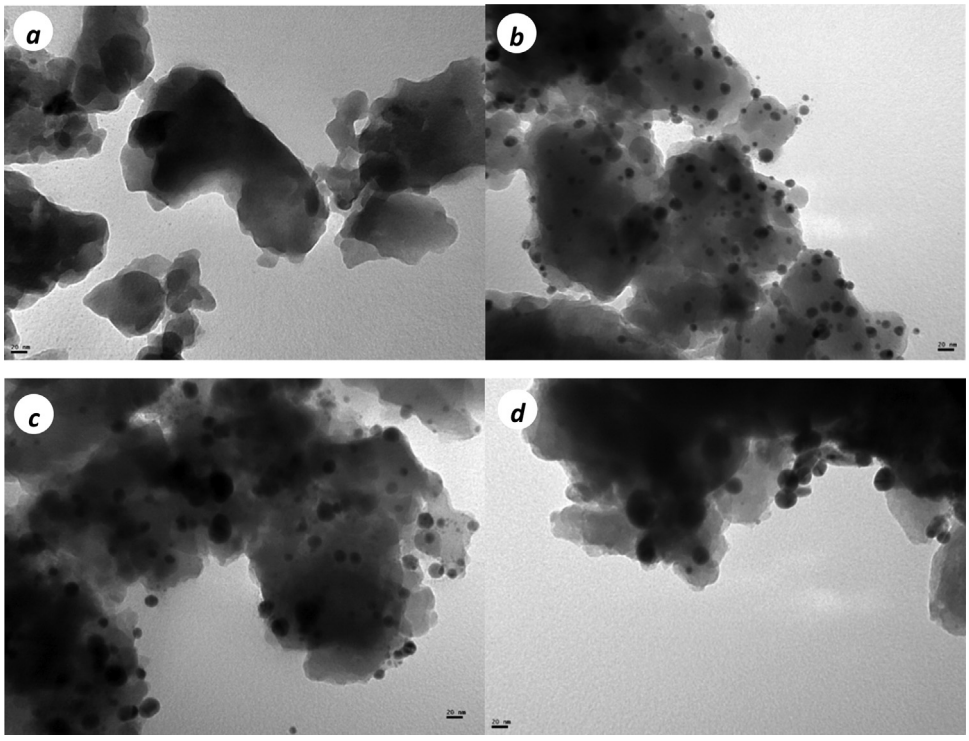

Fig. 2. TEM images for (a) Ag-free TMS-150 sample and silver containing (b) TMSAg-50, (c) TMSAg-150 and (d) TMSAg-450 samples. The size of the bars represents 20 nm in all the cases.

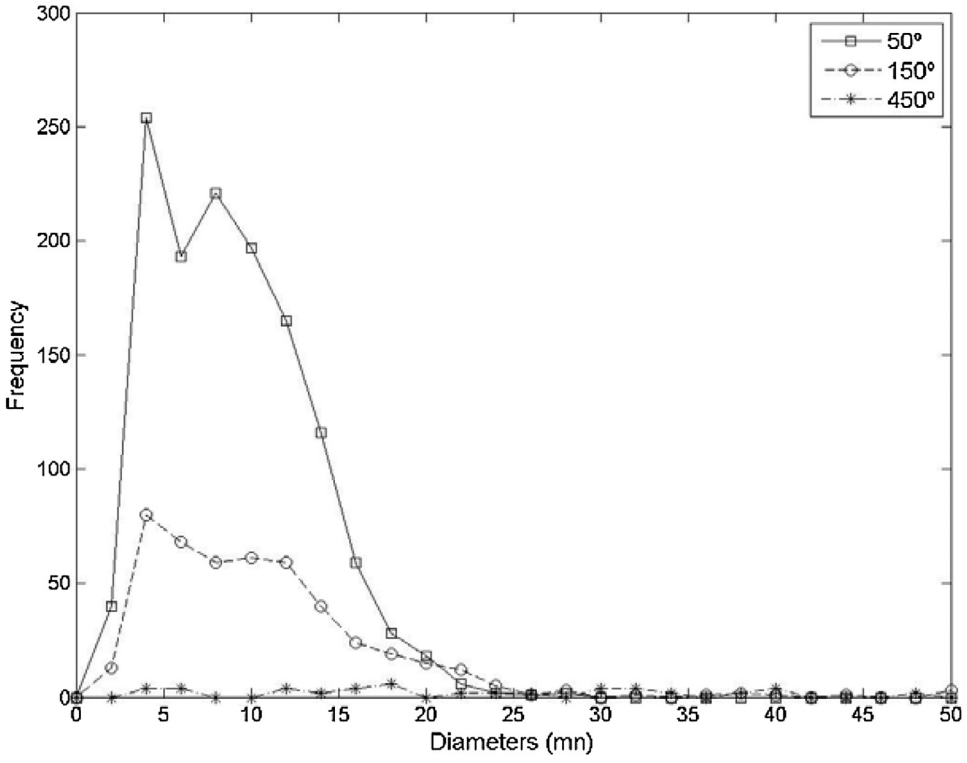

Fig. 3. Particle size distributions of silver nanoparticles developed for TMSAg samples at 50, 150 and 450 °C.

radiation source, Small Angle X-ray Scattering (SAXS) was performed to analyze the physical structure of the hybrid matrix as a function of the temperature of the thermal treatment. The developed coatings were also analyzed by Electrochemical Impedance Spectroscopy (EIS) and X-ray photoelectron spectroscopy (XPS), while the antibacterial behavior was studied through microbiological analysis by agar diffusion tests against *Escherichia coli* cultures.

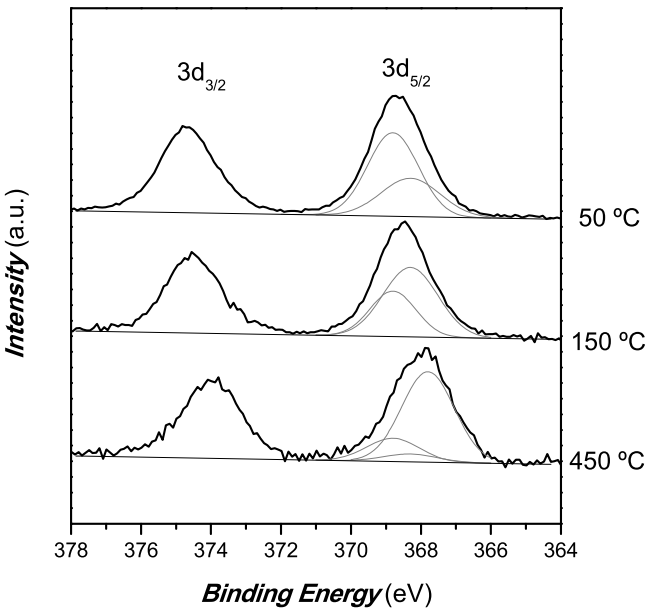

Fig. 4. Ag 3d XPS spectra of samples coated on microscope glass slides at 50, 150 and 450 °C of thermal treatment.

2. Materials and methods

2.1. Samples preparation

Hybrid sols were synthesized through the hydrolytic condensation of tetraethoxysilane (TEOS, 98%, Aldrich) and methyltriethoxysilane (MTES, 99%, Aldrich) in presence of silica nanoparticles (LUDOX® AS-40). Nitric acid (HNO_3 68%, Aldrich) was used as catalyzer. Silver doping was performed by the incorporation of a pyridine stabilized alcoholic solution of silver nitrate ($AgNO_3$, 99% Sigma-Aldrich) keeping a Ag/Si molar ratio of 3/97. The complete synthesis process was described in a previous work [27].

Alternatively, microscope glass slides and AISI 316L stainless steel plates were used as substrates. Coatings were deposited by the dip-coating method using a 2D PC-controlled system (FESTO Automation Engineering, Argentina). Plain substrates were immersed in the synthesized sol and then withdrawn at a constant speed of 25 cm/min. After a drying process at room temperature, 20 °C, samples were thermally treated at 50, 150 and 450 °C, calling them, respectively, TMAg-50, TMAg-150 and TMAg-450 samples. Also a silver-free (undoped) batch of samples, TM-50, TM-150 and TM-450 were prepared for the sake of comparison.

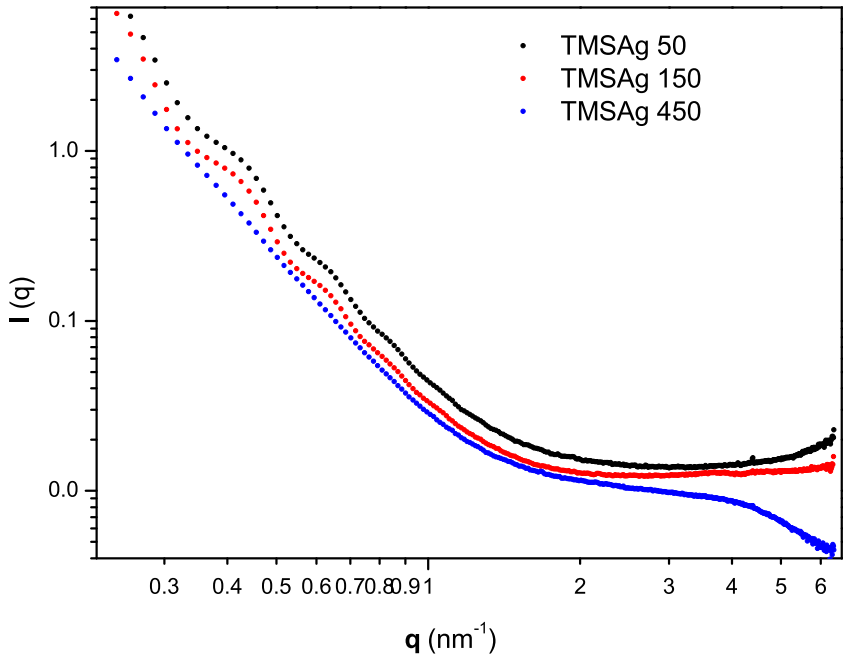

Fig. 5. Curves of Small Angle X-ray Scattering of silver loaded samples thermally densified at 50, 150 and 450 °C.

2.2. TEM

All samples were treated on mortar, dispersed with ethanol and placed into an ultrasonic bath for 15 min. Later, a drop of suspension was placed into 200 mesh grid (Formwar film). The observation was performed using a JEOL 100CX II Transmission Electronic Microscope (TEM) operating at 100 kV with 270000x working magnification. All samples were observed and analyzed at the same operation conditions.

2.3. Synchrotron SAXS

The structural evolution of the hybrid matrix was analyzed, as a function of the thermal treatment, by Small Angle X-ray Scattering (SAXS). The experiments were carried out using the SAXS1 beamline of the National Laboratory of Synchrotron Light (LNLS, Campinas, Brazil). Coatings were taken out from glass substrates by scratching. The resulting glassy powder was placed in the sample holders by adhesive polyimide film (Kapton®, DuPont). In order to subtract the contribution of the adhesive tape from SAXS patterns, Kapton® film was used as background. The collimated beam crossed the samples through an evacuated flight tube and was scattered to 2D bump-bonded hybrid-pixel Pilatus detector with an active area of 28 cm^2 and pixel size of 172×172 μm^2. The geometrical configuration was set up with the sample detector distance of 473.5 mm with monochromatic light of $\lambda = 1.55$ Å. The q range was calibrated with silver behenate, which has a well-known lamellar structure with d = 5.848 nm [29]. The isotropic 2D scattering patterns were collected after exposure times of 10 s. Images were corrected taking into account the detector dark noise and normalized by the sample transmission considering the 360 azimuthal scan. This procedure was carried out using the FIT2D software [30].

2.4. XPS

X-ray Photoelectron Spectroscopy (XPS) was performed using a VG Microtech ESCA3000 equipment to analyze the chemical neighbor of silver atoms as a function of the thermal treatment. A monochromatic Al Kα radiation of 1486.7 eV with a primary beam energy of 15 kV and an electron current of 5 A was used at Laboratório de Superfícies e Interfases (Universidade Federal do Paraná, Curitiba, Brazil). The base pressure inside the chamber was 3.10^{-10} mbar, and the spectra were performed close to 45° of take-off angle respect to the surface normal to the sample, using 0.8 eV of energy resolution for the hemispherical energy analyzer. The samples obtained on microscope glass slides were cut to fit into the instrument sample plate and were inserted into the chamber after 1 day of pressure stabilizing.

2.5. Electrochemical impedance spectroscopy

The electrochemical response of doped and undoped coated stainless steel (AISI 316L) was evaluated by means of Electrochemical Impedance Spectroscopy (EIS) measurements at room temperature (20 ± 1 °C) using a cylindrical three electrode electrochemical cell filled with 10–12 mL of naturally aerated and unstirred 0.35 wt.% NaCl solution prepared from p.a. grade chemicals (Sigma-Aldrich) and bidistilled water (Millipore, 18.2 MΩ cm). A $Hg/Hg_2Cl_2/KCl$ sat. (SCE, 244 mV vs. SHE by Radiometer Analytical, France) reference electrode and a Pt wire as auxiliary electrode were used. The stainless steel sheets served as working electrode and were mounted exposing an area of 3.464 cm^2 to the solution. EIS measurements were carried out using a potentiostat/galvanostat/ZRA Gamry Reference 600™. The EIS measurements were acquired applying a 5 mV_{rms} sinusoidal perturbation at 0 mV, from 50 kHz to 1 mHz and recording 10 points per frequency decade. The results were obtained immediately after mounting the electrochemical cell. Also, to substract any substrate contribution to the electrochemical response of EIS, AISI 316L was used as "blank" working electrode.

2.6. Agar diffusion tests

Overnight cultures of *E. coli* (K12 strain RP437) were diluted 1/50 and spread onto rich medium agar plates, containing 1% tryptone, 0.5% yeast extract, 0.5% NaCl and 1.3% agar. AISI 316L stainless steel plates with different coatings were placed on the agar surface and incubated at 37 °C for 24 h. The inhibitory activity was visualized as a clear halo between the coated plates and the bacterial lawn.

2.7. Determination of particle size distribution

Size distributions of silver nanoparticles were obtained through a mathematical algorithm, from TEM images, using techniques of digital image processing. The developed algorithm allows the detection and measurement of the diameters of these particles by a three-step process. Fig. 1 represents the process of the mathematical algorithm after every single step. In the first step particles were enhanced by a spectral band pass filter [31] using the following specifications: High pass 161, Low pass 21, Strength 3 and Passes 1. The result is a grayscale image where enhanced regions represent silver particles, Fig. 1b. This image shows a bimodal histogram which allows to determine a threshold value to discriminate the silver particles from the background. Then, as a second step, a binary image is obtained, Fig. 1c. In the third step the area and the center of mass of every particle present in the binary image is determined. Without loss of generality, it can be assumed that particles are spherical. So, in the third step, from the diameter obtained for each particle, the histogram corresponding to the size distribution of silver particles present in the image is obtained.

3. Results and discussions

Through the hydrolytic condensation of alkoxydes, homogeneous and colorless sols were synthesized and deposited by the dip-coating process on glassy and metallic substrates.

3.1. Development of silver nanoparticles

After thermal densifying treatments at 50, 150 and 450 °C, coatings remain homogeneous and crack-free showing a slightly yellow coloration at 150 °C and a light brown at 450 °C, but the silver-free coatings that kept its colorless independently of the thermal treatment. Those visually perceptible changes are the result of de development of silver nanoparticles within the hybrid structure of the sol-gel coating.

Observation through transmission electron microscopy, Fig. 2, reveals, as a first approach, a homogeneous dispersion of silver nanoparticles embedded in its clearer, with lower electronic density, surrounding matrix. When the thermal treatment rises, the ripening process of silver particles leads to the development of nanoparticles whose maximum size is highly related to the employed temperature. Through the analysis of particle size distribution by the developed mathematical algorithm, for all the analyzed samples, a wide dispersion of silver nanoparticles is observed, Fig. 3. Although this method is sensitive for particles higher than 5 nm diameter, approximately, it can be appreciated that with a thermal treatment of 50 °C a big amount of particles of up to near 20 nm are developed. When the thermal treatment reaches 150 °C the particle distribution spans up to near 30 nm with a considerable lower amount of particles. Finally, at 450 °C,

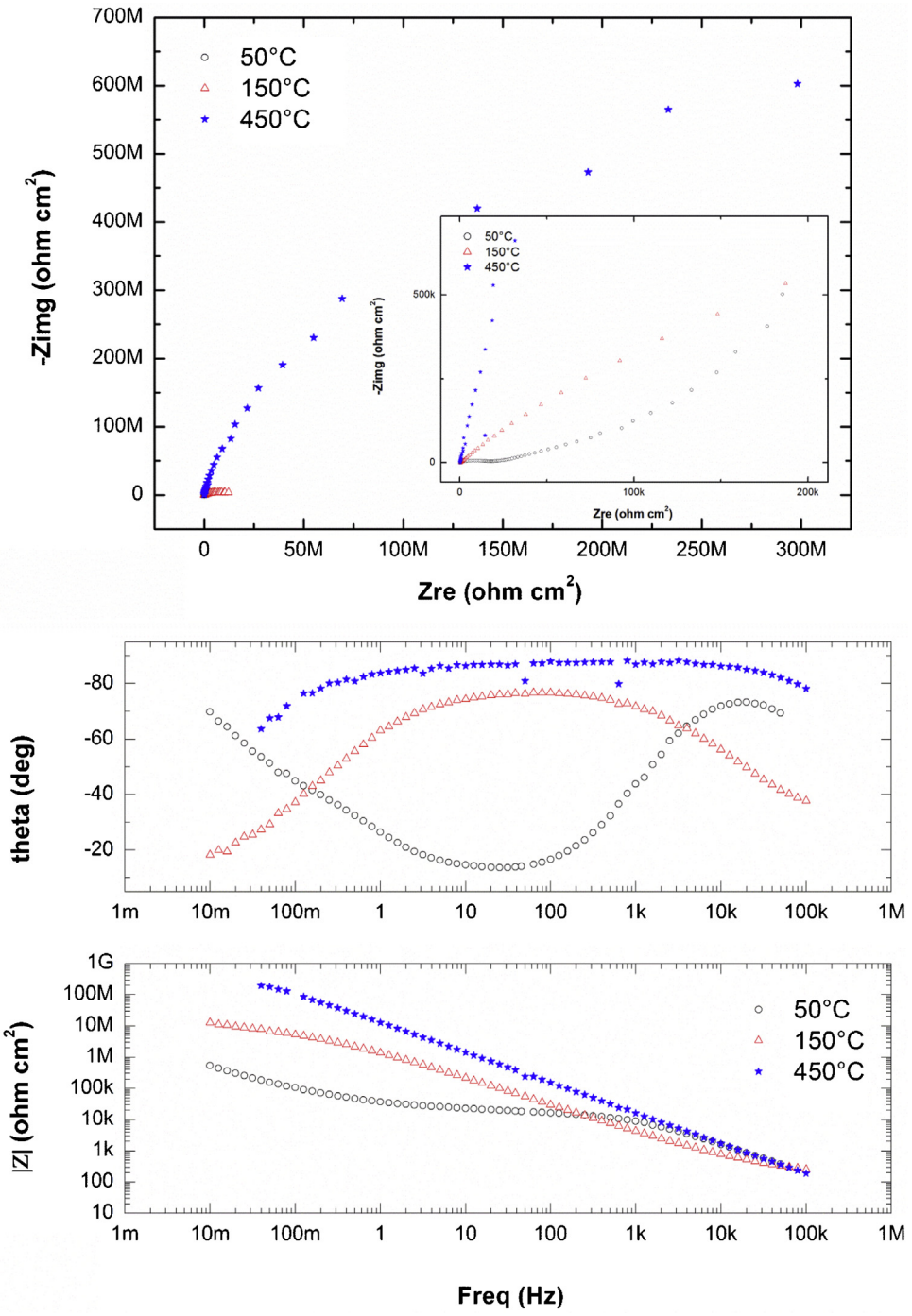

Fig. 6. EIS Nyquist and Bode plots for Ag-free coatings on 316L in contact with aerated 0.35% NaCl solution.

a flat distribution, with a near total absence of particles smaller than 10 nm is observed.

The general evolution of silver, from its ionic state as Ag^+, is accompanied by changes on its oxidative state. Fig. 4 shows the XPS spectra for silver in its 3d region and the deconvolution of the $3d_{5/2}$ peak in its components at 367.8, 368.3 and 368.8 eV corresponding, respectively, to Ag(III), Ag(0) and Ag(I) [32–34]. Table 1 shows the results of fittings presenting the relative area values for Ag $3d_{5/2}$ peaks. At 50 °C the XPS curve is dominated by Ag(I), attributed to $AgNO_3$, and a smaller component attributed to Ag(0). At 150 °C the proportion of metallic silver increases significantly in detriment of Ag(I). This evolution is in agreement with the results observed for TEM where pictures reveal the presence of silver nanoparticles with a clear growing from sample TMSAg-50 to TMSAg-150. At 450 °C (sample TMSAg-450) the signal of Ag(0) is strongly diminished and an intense peak of Ag(III) is developed at 367.8 eV. Both Ag(III) and Ag(I) are reported in literature as the components of AgO [32–35]. The overall evolution of silver through the thermal treatments results in a gradual loosening of Ag(I), generally accepted

Table 1
Relative area values, corresponding to 3d5/2 silver peaks, from XPS data fitting.

Sample	Ag(0)	Ag(I)	Ag(III)
TMSAg-50	0.348 ± 0.012	0.652 ± 0.011	–
TMSAg-150	0.647 ± 0.016	0.353 ± 0.016	–
TMSAg-450	0.064 ± 0.048	0.191 ± 0.028	0.745 ± 0.028

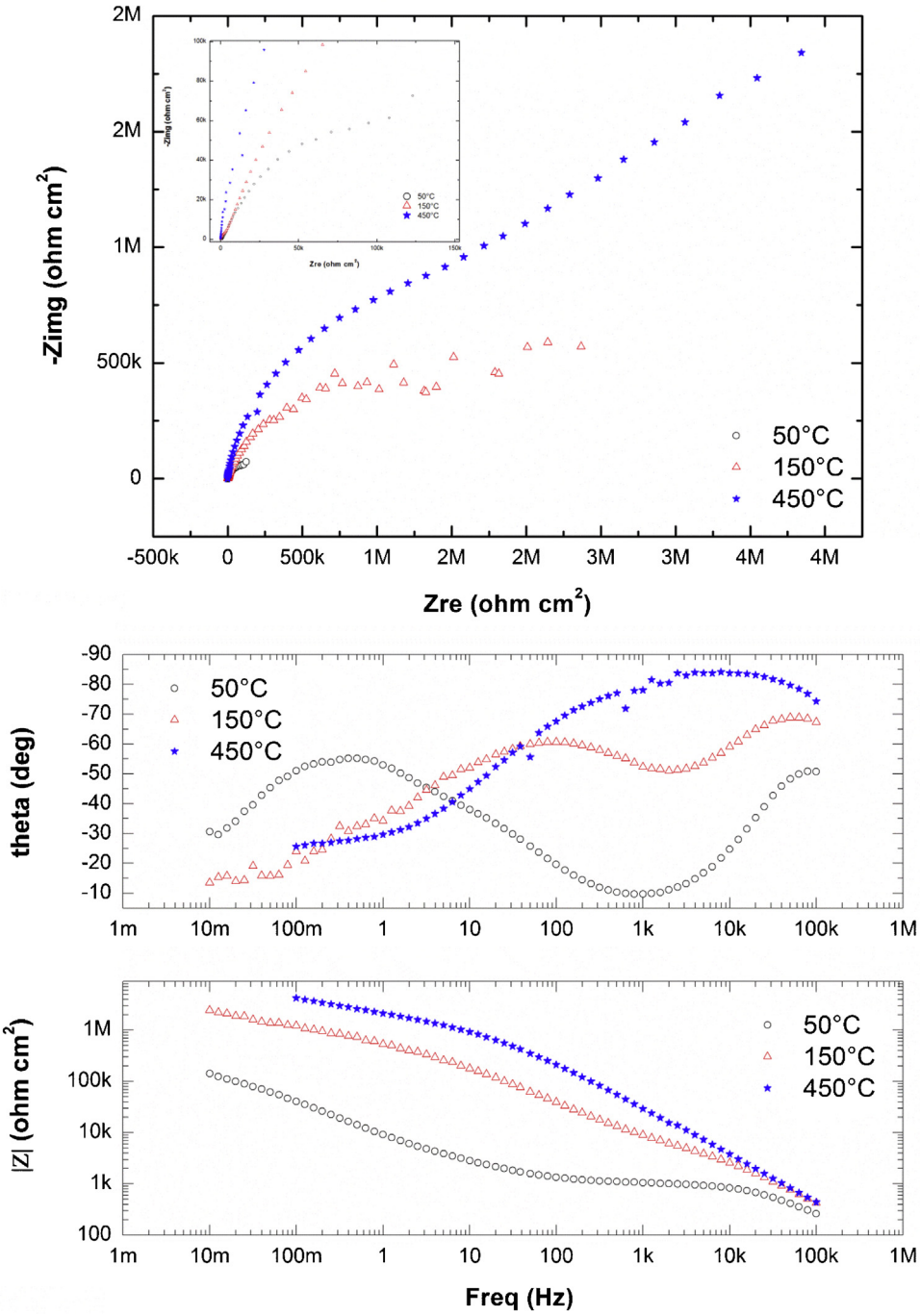

Fig. 7. EIS Nyquist and Bode plots for Ag-doped coatings on 316L in contact with aerated 0.35% NaCl solution.

as the main responsible of the antibacterial behavior of silver. Depending on the environmental conditions where the antibacterial material will work, i.e., immersed in an aqueous fluidic media or at the air atmosphere, the oxidative state of silver will be determinant of its efficiency against microorganisms. For instance, if a biocide material, based in metallic silver nanoparticles, is exposed to an aqueous media, a steady Ag^+ release could be reached from a superficial oxidative process with dissolved oxygen [36]. Then, the formation of silver nanoparticles observed for sample TMSAg-150, rich in Ag(0), could be a suitable supply of the antibacterial Ag^+ component for a long-term application.

Taking into account the spherical morphology of silver nanoparticles, that they are embedded in a hybrid matrix composed by a covalently bonded silica network, and the evolution of the aggregation state, the observed ripening process could be caused probably by an Ostwald ripening process more than a particles migration and coalescence mechanism, i.e., the atomic species transport from smaller particles and clusters to larger particles by diffusion through the matrix structure due to differences in its chemical potentials [37].

3.2. Structural evolution and electrochemical behavior

Thermal treatment also affects to the hybrid matrix. The analysis of the curves obtained by small angle X-rays scattering (SAXS), Fig. 5, in the region of $q > 4\ nm^{-1}$, reveals a gradual loosening of subnanometric structures, i.e., silver clusters and smallest components of the silica-based matrix, as isolated siloxanes, which, by effect of

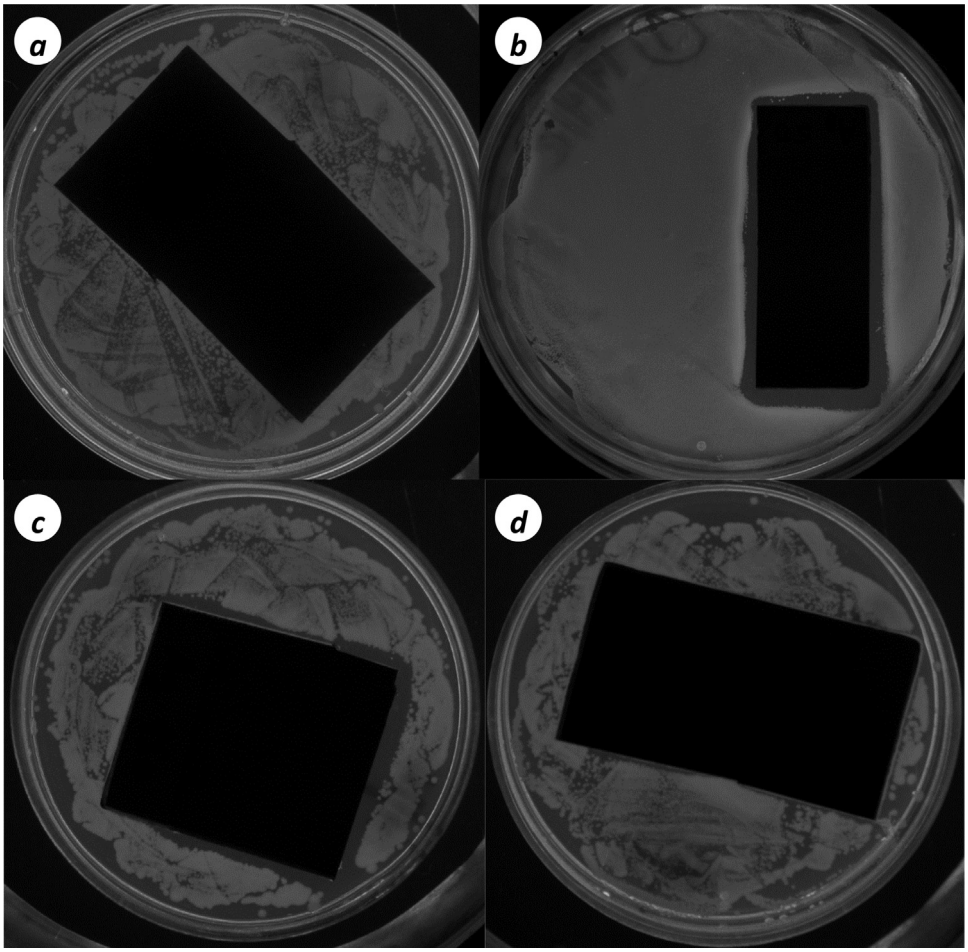

Fig. 8. Agar diffusion tests of stainless steel substrates coated with sol-gel hybrid materials on *Escherichia-Coli* cultures. (a) TMS-150, (b) TMSAg-50, (c) TMSAg-150 and (d) TMSAg-450. Petri dishes size: 50 mm.

thermal treatment, adhere to bigger structures. This observation is in agreement with the observed thought electron microscopy, where the smaller silver nanoparticles completely disappeared at 450 °C. Otherwise, in the region of the curves for $q < 2\,nm^{-1}$, it is clearly observed the effect of the thermal treatment on the hybrid structure of the matrix. At 50 °C a wavy curve is the result of a straight size distribution of silica nanoparticles. In previous works it was observed that the synthesis procedure of this kind of sols, with addition of silica nanoparticles, it rises an agglomeration of colloidal silica that carry to the formation of a monodisperse distribution of nanoparticles of 15 nm radius approximately [27]. The difference on the X-ray scattering length densities (SLD) between silica nanoparticles and the hybrid surrounding matrix allows its observation through SAXS experiments using a synchrotron radiation source. Since SLD is directly proportional to the mass density, and taking into account that silica nanoparticles are not able to diffuse, or to change its size distribution, inside the hybrid matrix, the vanishing of waviness observed on sample densified at 450 °C could be unequivocally attributed to an increasing of the bulk density of the hybrid matrix.

The electrochemical impedance analysis allows to estimate the evolution of the barrier properties of coatings, which could be assumed as a function of the network crosslinking of the matrix. In addition, some electrical parameters such as resistive and capacitive behavior of the coatings, adsorption, charge- and mass-transport, can be determined by using EIS. Fig. 6 shows the impedance diagrams in Nyquist and Bode representations for Ag-free coatings of TM-50, TM-150 and TM-450 after deposition on AISI 316L. A qualitative analysis of EIS diagrams shows a one time-constant due to the electrical double layer and a diffusive behavior for low thermal treatment (TT) samples (see Nyquist Fig. 6). As thermal treatment rises, a shift from a well-defined one time-constant system with a difusive low frecuency (LF) behavior to a wide two time-constants is shown on Bode representation, indicating a shift from resistive to capacitive behavior. This change is indicative of a strong blocking of electrolyte diffusion through the hybrid matrix as a result of a more densely crosslinked structure of the coating giving the so-called blocking electrode. In addition, at high frequencies (HF) no evidence of electrolyte solution response is observed due to total blocking of electrode surface, which is a northwoly point taking in account the protecting properties of these coatings.

A similar behavior is observed for the silver doped set of samples, but the region of resistive response is observed at higher frecuencies, as shown in Fig. 7. In addition, the change from resistive (for low TT) to capacitive (for high TT) response at high frequency (HF) observed for the Bode phase angle diagrams is indicative of a much more porous material obtained at lower TT. As TT rises the middle frequency range shows a wider phase angle response, indicating overlapping of time constants due to interaction between the substrate and the coating. Nyquist diagrams shows higher impedance as TT rises, evidencing better protective properties. Also, as for Ag-free samples, no electrolyte resistance is observed, indicating a good protective coating in all cases. The lower TT is applied the more porous coating was, which is coincident with results by SAXS spectroscopy for $q > 4$ nm-1, where silver sub-nanometric particles

and lower silica components migrate to the surface throughout a more open matrix.

3.3. Microbiological behavior

The antibacterial activity of samples was analyzed against *E.-Coli* through Agar Diffusion Tests. Fig. 8 shows the pictures of cultures after 24 h at 37 °C for the stainless steel plates coated with the hybrid materials. For TMS-150 sample, with no addition of silver, bacteria colonies grown independently from the presence of the sample, while for TMSAg-50, TMSAg-150 and TMSAg-450 the presence of an inhibitory halo was observed. A qualitative analysis of the size of such inhibitory halo allows determining a tight relationship with the thermal treatment at which samples were densified. The higher the densifying temperature, the lower the antibacterial activity. In fact, the antibacterial activity of TMSAg-450 sample is almost negligible; this behavior may be explained directly from the structural determinations that indicate, on one hand, the loosening of the smallest silver nanoparticles and the development of a highly crosslinked network of the hybrid matrix and, on the other hand, the lower availability of Ag(I). It is important to take in account that, although silver is present in a relatively low concentration and that the thickness of the coatings is about just 1.5 μm, a deeper study should be addressed taking in consideration the analysis of cytotoxicity of this kind of materials.

4. Conclusions

Hybrid organic-inorganic sol-gel coatings were synthesized from the hydrolytic condensation of TEOS and MTES in acidic media in presence of silica nanoparticles and deposited on AISI 316L stainless steel through the dip-coating method. Silver doping was carried out in the sol state by addition of an alcoholic solution of N-based stabilization of $Ag(NO)_3$.

As temperature of the densifying thermal treatment increases, Ag^+ ions reduce to Ag° forming metallic nanoparticles at 150 °C that become in AgO at higher temperatures, as it was seen at 450 °C from XPS experiments. This evolution in the oxidation state of silver is accompanied with an agglomeration process of silver nanoparticles, were the smaller nanoparticles trend to disappear at temperatures higher than 150 °C.

Incorporation of silver into the hybrid matrix introduces structural changes becoming in a much more permeable structure. Impedance spectroscopy showed a change from resisitive to capacitive behavior as thermal treatment rises, and a shift from a one time-constant behavior to a two time-constants, revealing a strong blocking of electrolyte diffusion through the hybrid matrix as a result of a more densely crosslinked structure of the coating as temperature of densification rises up.

As the temperature of thermal treatment increases, the electrolyte permeability diminishes and silver sub-nanometric particles grow. Those phenomena play an important role in silver diffusion and, then, in the biocide activity. Bacteriologic tests verified that the activity of silver-doped coatings against Escherichia coli cultures was stronger at lower temperatures of thermal densifying.

Acknowledgements

Authors want to acknowledge the Argentine National Council of Scientific and Technical Researches (CONICET, PIP 2012–0434), the Argentine National Agency of Scientific and Technological Promotion (ANPCyT, PICT-2011-0938) and the National Synchrotron Light Laboratory of Brazil (LNLS, Project 6780/10, proposal D11A-SAXS1-15291) for the financial supports. Also Dr. Wido H. Schreiner, LSI-LANSEN-UFPR, Brazil, is gratefully acknowledged for his helpful collaboration with XPS analysis.

References

[1] S.A. Jones, P.G. Bowler, M. Walker, D. Parsons, Wound Repair Regen. 12 (3) (2004) 288–294.
[2] S. Silver, L.T. Phung, Annu. Rev. Microbiol. 50 (1996) 753–789.
[3] J.H. Crabtree, R.J. Burchette, R.A. Siddiqi, I.T. Huen, L.L. Handott, A. Fishman, Perit. Dial. Int. 23 (4) (2003) 368–374.
[4] G. Zhao, S.E. Stevens, Biomaterials 11 (1998) 27–32.
[5] Y. Ando, H. Miyamoto, I. Noda, N. Sakurai, T. Akiyama, Y. Yonekura, T. Shimazaki, M. Miyazaki, M. Mawatari, T. Hotokebuchi, Mater. Sci. Eng. C 30 (1) (2010) 175–180.
[6] D. Zhang, G.W. Toh, H. Lin, Y. Chen, J. Mater. Sci. 47 (15) (2012) 5721–5728.
[7] H.J. Lee, S.Y. Yeo, S.H. Jeong, J. Mater. Sci. 38 (10) (2003) 2199–2204.
[8] M. Radetić, J. Mater. Sci. 48 (1) (2013) 95–107.
[9] A.M. El-Kady, A.F. Ali, R.A. Rizk, M.M. Ahmed, Ceram. Int. 38 (2012) 177–188.
[10] M.E. Rupp, T. Fitzgerald, N. Marion, V. Helget, S. Puumala, J.R. Anderson, P.D. Fey, Am. J. Infect. Control 32 (2004) 445–450.
[11] F. Furno, K.S. Morley, B. Wong, B.L. Sharp, P.L. Arnold, S.M. Howdle, R. Bayston, P.D. Brown, P.D. Winship, H.J.J. Reid, J. Antimicrob. Chemother. 54 (2004) 1019–1024.
[12] E. Falletta, M. Bonini, E. Fratini, N.A. Lo, G. Pesavento, A. Becheri, N.P. Lo, P. Canton, P. Baglioni, J. Phys. Chem. C 112 (2008) 11758–11766.
[13] B. Sun, S.Q. Sun, T. Li, W.Q. Zhang, J. Mater. Sci. 42 (24) (2007) 10085–10089.
[14] P. Jeanmonod, M.W. Laschke, N. Gola, M. von Heesen, M. Glanemann, M.D. Menger, M.R. Moussavian, Vasc. Endovascular Surg. 47 (6) (2014) 680–688.
[15] I. Ferreri, V. Lopes, S. Calderon, C.J. Tavares, A. Cavaleiro, S. Carvalho, Mater. Sci. Eng. C Mater. Biol. Appl. 42 (2014) 782–790.
[16] H. Qin, H. Cao, Y. Zhao, C. Zhu, T. Cheng, Q. Wang, X. Peng, M. Cheng, J. Wang, G. Jin, Y. Jiang, X. Zhang, X. Liu, P.K. Chu, Biomaterials 35 (33) (2014) 9114–9125.
[17] E. Charbel Abboud, J.C. Settle, T.B. Legare, J.E. Marcet, D.J. Barillo, J.E. Sanchez, Burns 40 (S1) (2014) 30–39.
[18] V. Dal Lago, L. Franca de Oliveira, K. Almeida Gonçalves, J. Kobarg, M.B. Cardoso, J. Mater. Chem. 21 (2011) 12267–12273.
[19] N. Li, L. Yongqian, L. Manqi, et al., J Mater. Sci. Mater. Med. 19 (2008) 3057–3062.
[20] R. Ling, N. Li, Y. Ke, Mater. Des. 32 (4) (2011) 2374–2379.
[21] I.T. Hong, C.H. Koo, Mater. Sci. Eng. A. 393 (1–2) (2005) 213–222.
[22] C.J. Brinker, G.W. Scherer, Sol–gel Science: The Physics and Chemistry of Sol–Gel Processing, Academic Press San Diego, California, USA, 1989.
[23] A.M. Vilardell, N. Cinca, A. Concustell, S. Dosta, I.G. Cano, J.M. Guilemany, J. Mater. Sci. 50 (13) (2015) 4441–4462.
[24] J. Ballarre, E. Jimenez-Pique, M. Anglada, S.A. Pellice, A.L. Cavalieri, Surf. Coat. Technol. 203 (2009) 3325–3331.
[25] B. Mahltig, D. Fiedler, H. Böttcher, J. Sol–Gel Sci. Technol. 32 (2004) 219–222.
[26] N. Stobie, B. Duffy, D.E. McCormack, J. Colreavy, M. Hidalgo, P. McHale, S.J. Hinder, Biomaterials 29 (2008) 963–969.
[27] R. Procaccini, S. Ceré, S. Pellice, Surf. Coat. Technol. 205 (2011) 5464–5469.
[28] R.A. Procaccini, C.A. Studdert, S.A. Pellice, Surf. Coat. Technol. 244 (2014) 92–97.
[29] T.C. Huang, H. Toraya, T.N. Blanton, Y. Wu, J. Appl. Crystallogr. 26 (2) (1993) 180–184.
[30] A.P. Hammersley, Scientific software FIT2D, European Synchrotron Research Facility Grenoble, 2009 http://www.esrf.eu/computing/scientific/FIT2D/.
[31] R.C. Gonzalez, R.E. Woods, Digital Image Processing, Vol. 1, Prentice Hall, Upper Saddle River, NJ, 2002.
[32] A.M. Ferraria, A.P. Carapeto, A.M. Botelho do Rego, Vacuum 86 (2012) 1988–1991.
[33] H.S. Shin, H.C. Choi, Y. Jung, S.B. Kim, H.J. Song, H.J. Shin, Chem. Phys. Lett. 383 (2004) 418–422.
[34] Y. Posada, J. Appl. Phys. 105 (2009), 126108–3.
[35] V.K. Kaushik, J. Elec. Spectrosc. Related Phenomena 56 (3) (1991) 273–277.
[36] L. Zhu, G. Lu, S. Mao, J. Chen, D.A. Dikin, X. Chen, R.S. Ruoff, NANO: Brief. Reports and Reviews 2 (3) (2007) 149–156.
[37] A.B.G. Lansdown, J. Wound Care 11 (4) (2002) 125–130.